Comparative analysis of absorbance calculations for integrated optical waveguide configurations by use of the ray optics model and the electromagnetic wave theory

Sergio B. Mendes and S. Scott Saavedra

Focusing on the use of planar waveguides as platforms for highly sensitive attenuated total reflection spectroscopy of organic thin films, we extend the ray optics model to provide absorbance expressions for the case of dichroic layers immobilized on the waveguide surface. Straightforward expressions are derived for the limiting case of weakly absorbing, anisotropically oriented molecules in the waveguide–cladding region. The second major focus is on the accuracy of the ray optics model. This model assumes that the introduction of absorbing species, either in the bulk cladding or as an adlayer on the waveguide surface, only causes a small perturbation to the original waveguide-mode profile. We investigate the accuracy of this assumption and the conditions under which it is valid. A comparison to an exact calculation by use of the electromagnetic wave theory is implemented, and the discrepancy of the ray optics model is determined for various waveguide configurations. We find that in typical situations in which waveguide-absorbance measurements are used to study organic thin films ($k_l/n_l \leq 10^{-1}$, $h/\lambda \approx 10^{-2}$) the discrepancy between the ray optics and the exact calculations is only a few percent (2–3%). © 2000 Optical Society of America

OCIS codes: 300.6490, 240.6490, 230.7390, 130.3120, 240.0310, 240.6690.

1. Introduction

Monolayers of organic molecules with a thickness of a few nanometers have been a subject of increasing interest in recent years, as reported in the critical review of Swalen *et al.*[1] Potential technological applications of these films include optical and electronic devices, sensors, and biomaterial surfaces.[2–5] To exploit these possibilities fully, it is necessary to address several challenging problems. Among them are relations between the structural and the functional properties of molecules deposited as a very thin film on a solid support. The investigation of these relations is a technically difficult challenge because of the high sensitivity required for monolayer detection, which should also be combined with nondestructive

sampling and *in situ* analysis. It has been demonstrated[6–8] that the planar optical waveguide offers a highly sensitive platform for spectroscopically probing organic films in the submonolayer regime. Applications include self-assembled films, polymers, Langmuir–Blodgett films, chemical sensor layers, organic dye films, and protein monolayers.[9–22] The inherent sensitivity of waveguide-absorbance measurements to the broadband spectral regime are extended with the recent development of a multichannel, single-mode, planar waveguide-based spectrometer.[23]

For mathematical analysis of waveguide structures that comprise lossy media, as in the case of an absorbing layer or cladding on a waveguide surface, we find in the literature several approaches. These can be broadly classified as exact and approximate. Among the exact approaches for the calculation of the attenuation coefficient is early research on solutions for simple cases, as in that performed by Burke[24] who produced a graphical solution for the symmetric, three-media, lossy waveguide in the TE polarization. The extension to asymmetric configurations, TM modes, and automatic computer calculation was described by Kaminow *et al.*[25] The application of the

The authors are with the University of Arizona, 1630 East University Boulevard, Tucson, Arizona 85721. S. B. Mendes (sergiom@u.arizona.edu) is with the Optical Sciences Center. S. Scott Saavedra is with the Department of Chemistry.

transfer-matrix method to multilayer waveguides and the subsequent solution of a root-finding problem to determine the waveguide-bound modes have dominated recent research. Such procedures can be found in Chilwell and Hodgkinson[26] and Offersgaard.[27] An interesting alternative for solving the eigenvalue problem has been given by Ghatak *et al.*[28] by introduction of a prism coupler and by scanning of the coupling angle to find the resonant eigenvalues of a multilayer waveguide structure. The integral approach taken by Li[29] guarantees calculation of all bound modes.

Different approximate approaches have been pursued to provide direct expressions of the attenuation coefficient in specific lossy waveguide structures. A complex index of refraction has been assumed in the waveguide-characteristic equation for particular cases and limits.[30,31] Another approach, which is frequently employed in optical fiber configurations, is the perturbation analysis.[32–35] In this technique, the waveguide loss is calculated by the fraction of the modal power inside the absorbing region. Stewart and Culshaw[36] used a ray optics approach and the Fresnel reflection coefficient to describe the case of bulk-cladding absorption in the waveguide configuration at the TE polarization.

Our focus here is twofold. First, absorbance calculations in waveguide structures with the ray optics model are extended to thin dichroic layers of chromophores. This extension is important for studies of molecular films in which waveguide-based attenuated total reflection spectroscopies are used. Specifically, the orientation distribution of the molecules in a film can significantly affect the functional properties of the ensemble, and orientation–function relations in molecular films are being studied with waveguide attenuated total reflection techniques in several laboratories. The derivations presented here yield straightforward expressions for the limiting case of weakly absorbing, anisotropically oriented ensembles of molecules in the waveguide-cladding region for both the TE and the TM polarizations. In addition, these derivations correct an error in published expressions[37] of the dichroic ratio obtained from waveguide-based attenuated total reflection measurements.

Our second major focus is the accuracy of the ray optics model. This model, as well as the other approximate approaches discussed above, assumes that the introduction of absorbing species either in the bulk cladding or as an adlayer only causes a small perturbation to the original waveguide-mode profile. The accuracy of this assumption has not been considered in detail. Here we assess the accuracy of this assumption and the conditions under which it is valid by performing a comparison of absorbance calculations using approximate (ray optics) and exact approaches for typical waveguide configurations. For exact calculations, we employ the method of Offersgaard[27] because it provides a convenient extension of the electromagnetic wave-vector theory to eigenvalue calculation of the propagating guided modes in

waveguide structures containing dichroic or birefringent layers.

2. Wave Model

In the wave model the waveguide structure is treated as a multilayer stack with each layer characterized by a thickness t and a dielectric constant tensor $\bar{\varepsilon}$. A diagonal tensor, where all nondiagonal components are nulls, is used in the analysis. More general descriptions of the dielectric constant are straightforward; however, the experimental situations to be addressed here can be fully described by the diagonal tensor represented in Eq. (1).

$$\bar{\varepsilon} = \varepsilon_0 \begin{pmatrix} n_x{}^2 & 0 & 0 \\ 0 & n_y{}^2 & 0 \\ 0 & 0 & n_z{}^2 \end{pmatrix}, \tag{1}$$

where ε_0 is the vacuum dielectric constant.

For an isotropic layer, the three diagonal tensor components are equal. A dichroic or birefringent layer is represented by a tensor with unequal diagonal elements. In particular the dichroism is described by different values of the imaginary part of the complex refractive index $n_\alpha - ik_\alpha$, with $\alpha = x, y$, and z.

The bound modes of the multilayer waveguide structure are derived from Maxwell's equations and boundary conditions. A transfer-matrix approach is used in the calculation of the tangential vector components of the electric and magnetic fields. By imposing on the resulting fields a bounding-mode condition, a characteristic waveguide equation is obtained, as described by Offersgaard.[27] Next the effective indices of the guided modes are obtained from the characteristic waveguide equation by a Muller's numerical procedure[38] implemented in an automatic computer routine. The numerical error of this procedure can be made extremely small with conventional personal computers and certainly much smaller than any experimental accuracy. When at least one absorbing material is present in the waveguide structure, the resulting effective index is a complex number, $\tilde{N} = N_{\text{Re}} - iN_{\text{Im}}$, with its imaginary component determining the attenuation of the propagating mode. In absorbance units, the attenuation is given by

$$A = \frac{4\pi L}{\lambda \ln 10} N_{\text{Im}}, \tag{2}$$

where L is the propagation length of the guided mode and λ is the free-space wavelength.

3. Ray Optics Model

Unlike the electromagnetic wave approach, which includes at the outset the absorbing media in the calculation, the ray optics model first assumes a lossless waveguide structure. The effective refractive index, N, and the effective thickness, t_{eff}, of each guided mode are calculated for the lossless structure. Next, absorbing species are introduced as a small pertur-
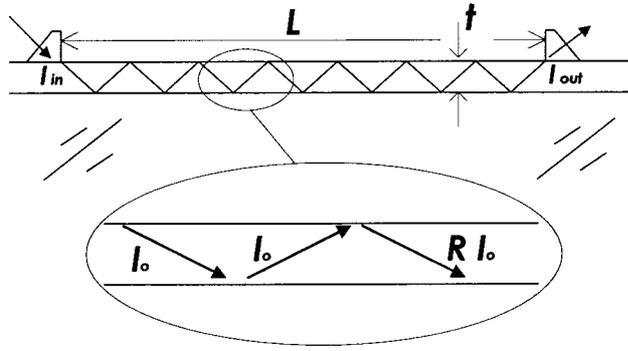
Fig. 1. Schematic representation of the waveguide configuration treated with the ray optics model. Total internal reflection is frustrated at the waveguide–cladding interface.

bation. Either a small extinction coefficient is introduced into the cladding material or a thin absorbing layer is introduced between the waveguide and the cladding. A critical assumption is that the perturbation is small enough so that the previously calculated quantities, N and t_{eff}, can be used in the equations to follow. The calculation of the attenuation coefficient, or absorbance, is straightforward. The introduction of an absorbing medium frustrates the total internal reflection at the waveguide–cladding interface, as indicated in Fig. 1. The attenuation of the propagating guided mode can then be described by the intensity reflection coefficient, R, at the waveguide–cladding interface. If we define η as the total number of reflections at the waveguide–cladding interface, then the absorbance can be written as

$$A = -\log_{10}(R^{\eta}) \cong \frac{\eta(1 - R)}{\ln 10}, \qquad (3)$$

where we have used the weak perturbation assumption ($R \cong 1$). The total number of reflections calculated from the ray optics model is given by

$$\eta = \frac{(n_w{}^2 - N^2)^{1/2}}{2N} \frac{L}{t_{\text{eff}}}, \qquad (4)$$

where n_w is the waveguide index of refraction. The expression of the waveguide effective thickness, t_{eff}, which takes into account the Goos–Hänchen shift effects,[31] is given by

$$t_{\text{eff,TE}} = t + \frac{\lambda/2\pi}{(N_{\text{TE}}^2 - n_c{}^2)^{1/2}} + \frac{\lambda/2\pi}{(N_{\text{TE}}^2 - n_s{}^2)^{1/2}}, \qquad (5)$$

for the TE polarization, where n_c and n_s are the refractive index of cladding and substrate, respectively, and t is the waveguide thickness.[39] For the TM polarization the effective thickness is given by

$$t_{\text{eff,TM}} = t + \frac{\lambda/2\pi}{q_c(N_{\text{TM}}^2 - n_c{}^2)^{1/2}} + \frac{\lambda/2\pi}{q_s(N_{\text{TM}}^2 - n_s{}^2)^{1/2}}, \qquad (6)$$

where

$$q_{c,s} \equiv \left(\frac{N_{\text{TM}}}{n_w}\right)^2 + \left(\frac{N_{\text{TM}}}{n_{c,s}}\right)^2 - 1. \qquad (7)$$

The intensity reflection coefficient, R, is the sole parameter that remains to be determined for the absorbance calculation in Eq. (3).

Before presenting the results for particular waveguide configurations, a few comments and definitions may be helpful. For calculations presented here the imaginary part of the index of refraction, k, also known as the extinction coefficient is used. This quantity is related to the molar absorptivity, ε, and the molar concentration, c, by the following expression:

$$\frac{4\pi k}{\lambda \ln 10} = \varepsilon c. \qquad (8)$$

In close analogy with Beer's law we define the equivalent pathlength, b_{wg}, in a waveguide experiment by means of

$$b_{\text{wg}} \equiv \frac{A}{\varepsilon c}. \qquad (9)$$

The equivalent pathlength describes the waveguide response, which, when combined with the material optical response, εc, provides the absorbance measured in a waveguide platform. This quantity is related to Harrick's[40,41] definition of evanescent pathlength, d_e, by

$$b_{\text{wg}} = \eta d_e. \qquad (10)$$

Thus the key parameter to describe the absorbance measured in a waveguide is the product of the number of reflections, η, and the evanescent pathlength, d_e. We emphasize that once the expression for b_{wg} is determined, the absorbance can be easily calculated from Eq. (9). In other words, b_{wg} contains all the information regarding the waveguide mode that affects the absorbance, i.e., the intensity of the electric field at the cladding interface, the evanescent depth of penetration, the effective index of refraction, and the wavelength dependence (modal and material dispersion) of all these parameters. Therefore, in the remaining part of this section, we present the expressions of the equivalent pathlength for waveguide configurations of interest. First, the case of a bulk absorbing cladding media is considered. Next, both isotropic and dichroic absorbing layers deposited on the waveguide surface are examined.

A. Bulk Absorbance

A waveguide with an absorbing cladding medium is illustrated in Fig. 2. By using the Fresnel reflection coefficient at the waveguide–cladding interface and taking the limiting case of a weakly absorbing medium, $(k_c/n_c) \ll 1$, one calculates the intensity reflection coefficient, R, for each polarization. Inserting this result into Eq. (9) yields the following
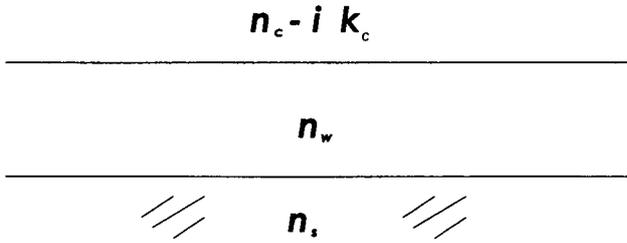
$$n_c - i\,k_c$$

$$n_w$$

$$n_s$$

Fig. 2. Schematic representation of the waveguide structure with an absorbing cladding medium.

expressions for the equivalent pathlength in the case of a bulk absorbing medium, $b_{b,\mathrm{wg}}$, in each polarization: for TE modes,

$$b_{b,\mathrm{wg}} = \left[\frac{\lambda}{4\pi(N_{\mathrm{TE}}^2 - n_c^2)^{1/2}}\right]\left\{\frac{2n_c(n_w^2 - N_{\mathrm{TE}}^2)}{t_{\mathrm{eff,TE}}N_{\mathrm{TE}}(n_w^2 - n_c^2)}L\right\}, \tag{11}$$

and for TM modes,

$$b_{b,\mathrm{wg}} = \left[\frac{\lambda}{4\pi(N_{\mathrm{TM}}^2 - n_c^2)^{1/2}}\right]$$
$$\times \left\{\frac{2n_c n_w^2(n_w^2 - N_{\mathrm{TM}}^2)(2N_{\mathrm{TM}}^2 - n_c^2)}{t_{\mathrm{eff,TM}}N_{\mathrm{TM}}[n_w^4(N_{\mathrm{TM}}^2 - n_c^2) + n_c^4(n_w^2 - N_{\mathrm{TM}}^2)]}L\right\}. \tag{12}$$

As seen in Eqs. (11) and (12), the equivalent pathlength in both TE and TM polarization is proportional to the depth of penetration, which appears inside the square brackets.

B. Isotropic Adlayer Absorbance

A schematic representation of the absorbance due to an adlayer of thickness h and refractive index $n_l - ik_l$ deposited on the waveguiding film is shown in Fig. 3, assuming $k_x = k_y = k_z = k_l$. The ray optics model assumes a weakly absorbing medium $(k_l/n_l) \ll 1$ and a very thin layer $(h/\lambda) \ll 1$. Under these assumptions, the intensity reflection coefficient of the waveguide–adlayer–cladding system is calculated,

$$n_c$$

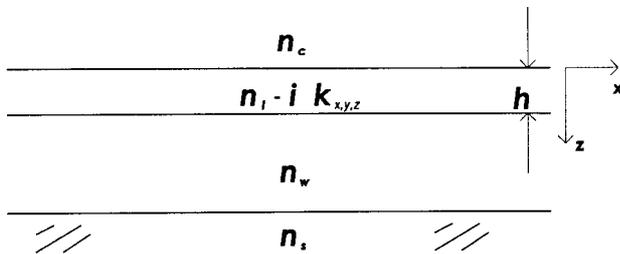$$n_l - i\,k_{x,y,z} \qquad h$$

$$n_w$$

$$n_s$$

Fig. 3. Schematic representation of the waveguide structure with an absorbing dichroic adlayer on the upper surface of the guiding film. Also indicated is the adopted coordinate system.

as by Macleod,[42] to determine the equivalent pathlength, $b_{l,\mathrm{wg}}$, in each polarization: for TE modes,

$$b_{l,\mathrm{wg}} = h\left\{\frac{2n_l(n_w^2 - N_{\mathrm{TE}}^2)}{t_{\mathrm{eff,TE}}N_{\mathrm{TE}}(n_w^2 - n_c^2)}L\right\}, \tag{13}$$

and for TM modes,

$$b_{l,\mathrm{wg}} = h$$
$$\times \left\{\frac{2n_l n_w^2(n_w^2 - N_{\mathrm{TM}}^2)[(1 + (n_c/n_l)^4)N_{\mathrm{TM}}^2 - n_c^2]}{t_{\mathrm{eff,TM}}N_{\mathrm{TM}}[n_w^4(N_{\mathrm{TM}}^2 - n_c^2) + n_c^4(n_w^2 - N_{\mathrm{TM}}^2)]}L\right\}, \tag{14}$$

Equations (13) and (14) show that the equivalent pathlength is proportional to the adlayer thickness, h. The proportionality constant is identical to that in Eqs. (11) and (12), assuming that $n_c = n_l$. The adlayer absorbance is proportional to the adlayer thickness in the same proportion that the bulk absorbance is related to the depth of penetration.

C. Dichroic Adlayer Absorbance

Next we consider the absorbance in each polarization due to a dichroic adlayer deposited on the waveguide surface with the optical constant as indicated in Fig. 3. The calculation of the extinction coefficient in each Cartesian direction, $k_{x,y,z}$, from the molecular dipole orientation is described in Appendix A. The intensity reflection coefficient of the waveguide–adlayer–cladding system follows the analysis reported by Macleod,[42] with the anisotropic coefficients taken from Horowitz and Mendes.[43] Assuming a thin and weakly absorbing adlayer, as before, the following equivalent pathlength is obtained: for TE modes,

$$b_{l,\mathrm{wg}} = h\,\frac{2n_l f_y(n_w^2 - N_{\mathrm{TE}}^2)}{t_{\mathrm{eff,TE}}N_{\mathrm{TE}}(n_w^2 - n_c^2)}L, \tag{15}$$

and for TM modes,

$$b_{l,\mathrm{wg}} = h$$
$$\times \frac{2n_l n_w^2(n_w^2 - N_{\mathrm{TM}}^2)[(N_{\mathrm{TM}}^2 - n_c^2)f_x + (n_c/n_l)^4 N_{\mathrm{TM}}^2 f_z]}{t_{\mathrm{eff,TM}}N_{\mathrm{TM}}[n_w^4(N_{\mathrm{TM}}^2 - n_c^2) + n_c^4(n_w^2 - N_{\mathrm{TM}}^2)]}L, \tag{16}$$

where the factor f_i, defined in Appendix A, is the ratio between the extinction coefficient along a coordinate axis and the extinction coefficient for a random molecular orientation. In the isotropic limit we have $f_x = f_y = f_z = 1$, and Eqs. (15) and (16) reduce to Eqs. (13) and (14), respectively.

Note that the equivalent pathlength, as described in Eqs. (11)–(16), incorporates both explicit and implicit wavelength dependencies. Therefore absorption spectra performed in a waveguide configuration may exhibit differences from the corresponding spectra obtained in a transmission configuration. A direct comparison of the spectra may incorrectly suggest spectral shifts that are simply related to the wavelength dependence of the waveguide mode. It

is important to consider these dispersion effects in any spectral analysis before attempting to draw valid conclusions. This observation is especially important in applications of waveguide spectroscopy in which observed spectral shifts are interpreted in terms of the microenvironment of the chromophores in the waveguide adlayer.

4. Comparison Analysis

In this Section, the electromagnetic-wave approach and the ray optics model are compared. The validity of the ray optics model and its weak perturbation assumptions are assessed for typical waveguide configurations.

A. Bulk Absorption

First we consider a Corning 7059 glass waveguide ($n_w = 1.56$, $t = 400$ nm) deposited on a fused-silica substrate ($n_s = 1.46$). The cladding material is an aqueous solution in which absorbing species are dissolved. The optical constants assumed for the solution are $n_c = 1.33 - ik_c$. For each value of k_c, the absorbance is calculated with both the full-wave model of Section 2 and the ray optics model with Eqs. (11) and (12). The wavelength for the calculations was 550 nm. Figure 4(a) shows the calculated waveguide absorbance per unit length of mode propagation along the guide, A_{wg}/cm, plotted against the extinction coefficient of the cladding solution, k_c. As seen in the plot, the ray optics and the wave models show no significant difference at low to moderate values of the extinction coefficient, demonstrating agreement between the two approaches. However, at high values of k_c, small deviations between the two approaches are observed as expected since the assumption for the derivation of the ray optics model ($k_c/n_c \ll 1$) is no longer valid. These deviations are illustrated in Fig. 4(b) where the relative error is plotted; the relative error is defined as the difference between the absorbance values calculated with the ray optics and the wave models, divided by the absorbance of the wave model. For $k_c = 0.001$, which corresponds to A_{wg}/cm values of 3 (TE) and 5 (TM), the discrepancy between the two calculations is only approximately 0.01%. Thus for experimentally measurable A_{wg} values, the ray optics model is an accurate approximation.

B. Isotropic Adlayer Absorption

Next we examine a thin absorbing adlayer deposited on the upper surface of two waveguide configurations. The first configuration is the same waveguide as described above: a Corning 7059 glass film ($n_w = 1.56$, $t = 400$ nm) deposited on a fused-silica substrate ($n_s = 1.46$). The cladding media is water ($n_c = 1.33$), and the wavelength is 550 nm. The adlayer is a 3-nm-thick film, which is a typical value for a protein monolayer.[15] The real part of the refractive index of the adlayer is assumed the same as the water superstrate ($n_l = n_c = 1.33$). The extinction coefficient, k_l, for the adlayer is considered over the range from 0 to 0.1. The relation between molar
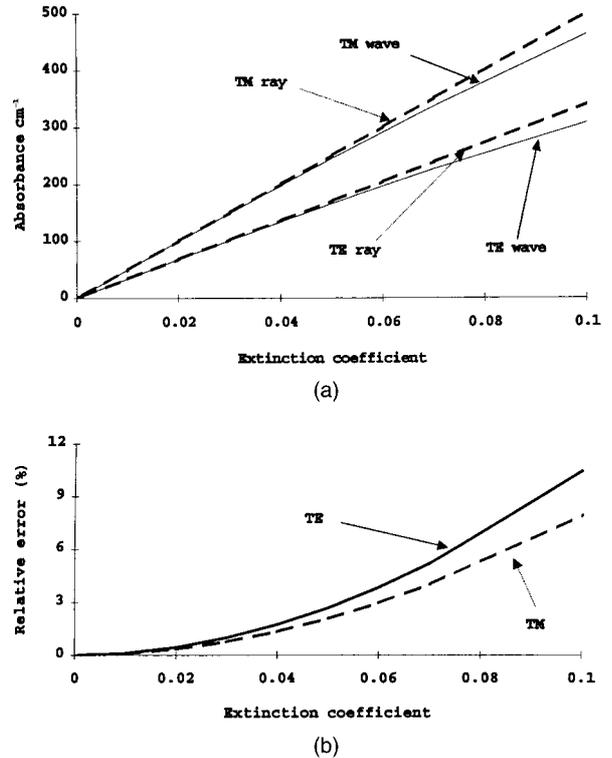

(a)

(b)

Fig. 4. Calculations for a bulk absorbing cladding medium with a variable extinction coefficient, k_c. (a) Absorbance values calculated with the ray optics (dashed lines) and the wave (solid lines) models. (b) Relative error of the ray optics model compared with the wave model calculation. The parameters used in the calculations are wavelength $\lambda = 550$ nm, waveguide thickness $t = 400$ nm, waveguide index of refraction $n_w = 1.56$, substrate index of refraction $n_s = 1.46$, and real part of cladding index of refraction $n_c = 1.33$.

absorptivity and extinction coefficient in the case of a molecular layer should be noted. For a molecule with a cross-sectional area of 9 nm^2, a single monolayer corresponds to a surface coverage of 1.85×10^{-11} moles/cm^2. For this case, an extinction coefficient of 0.1 corresponds to a molar absorptivity of $161,000\ M^{-1}\ cm^{-1}$. Thus the range of 0 to 0.1 for the extinction coefficient covers a broad range of molar absorptivity and surface coverage.

In Fig. 5(a) the results calculated with the ray optics model are compared with those from the exact full-wave approach. The discrepancy between the two approaches is expressed as the relative error, as defined above, and is plotted in Fig. 5(b). The relative error is approximately 2% over a broad range of the extinction coefficient.

Next we examine a different single-mode waveguide configuration with $n_w = 1.80$ and $t = 180$ nm, keeping all other variables constant. A tightly confined waveguide (relative to the 7059 waveguide) was chosen to determine if the degree of mode confinement has any effect on the accuracy of the ray optics model. The calculated relative error is plotted in Fig. 6. The discrepancy of the ray optics model with respect to the full-wave model is approximately only 3%.
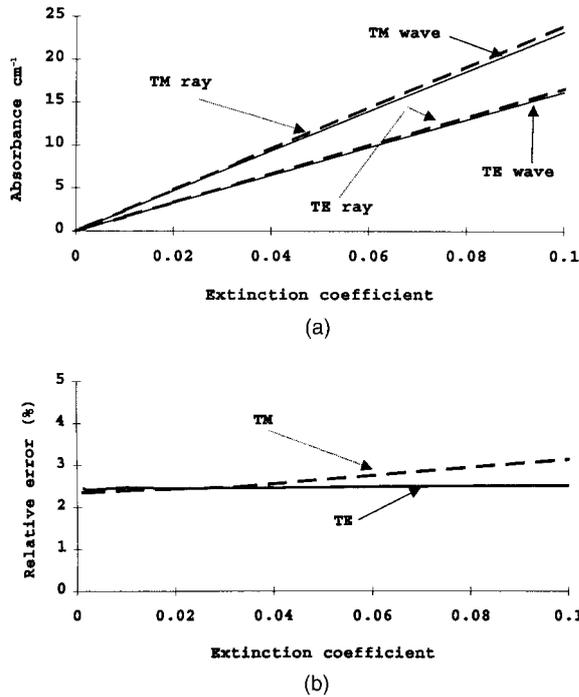
(a)

(b)

Fig. 5. Calculations for an isotropic absorbing adlayer with a variable extinction coefficient, k_l. (a) Absorbance values calculated by the ray optics (dashed lines) and the wave (solid lines) models. (b) Relative error of the ray optics model compared with the wave model calculation. The parameters used in the calculations are wavelength $\lambda = 550$ nm, waveguide thickness $t = 400$ nm, waveguide index of refraction $n_w = 1.56$, substrate index of refraction $n_s = 1.46$, real part of the adlayer index of refraction $n_l = 1.33$, and cladding index of refraction $n_c = 1.33$.

C. Dichroic Adlayer Absorption

Next the ray optics model and the full-wave approach are compared for a thin dichroic absorbing adlayer deposited on the upper surface of a waveguide. The same glass waveguide structure described above is considered: a fused-silica substrate ($n_s = 1.46$), a Corning 7059 glass film ($n_w = 1.56$, $t = 400$ nm), and water ($n_c = 1.33$) as the cladding material. The dichroic adlayer is modeled as a 3-nm-thick film with a complex and anisotropic refractive index of $1.33 -$
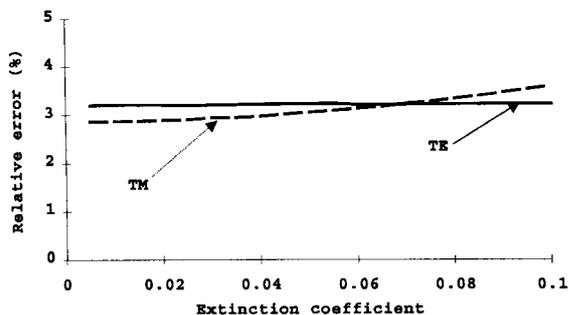

Fig. 6. Relative error of the ray model compared with the wave model for an absorbing adlayer. The waveguide configuration is the same as described in Fig. 5, except for waveguide thickness $t = 180$ nm and waveguide index of refraction $n_w = 1.80$.

$ik_{x,y,z}$. The film is composed of molecules having a linear electronic absorption dipole, as described in the Appendix A.1. A rotationally symmetric distribution is assumed for the dipole orientation distribution in the waveguide plane (the x–y plane in Fig. 3). The dichroism is due to a nonrandom distribution in the polar angle θ, which is the angle between the electronic absorption dipole and the axis perpendicular to the waveguide surface (z axis). Each Cartesian component of the extinction coefficient can then be written in terms of the extinction coefficient, k, for the isotropic case and the mean tilt orientation angle, $\bar{\theta}$, by use of

$$k_x = k_y = \tfrac{3}{2} k \, \sin^2(\bar{\theta}), \tag{17}$$

$$k_z = 3k \, \cos^2(\bar{\theta}). \tag{18}$$

The isotropic condition ($k_x = k_y = k_z = k$) occurs at the magic angle, $\bar{\theta} = 54.74°$.

The absorbance in the TE and the TM polarizations are calculated as the tilt orientation angle $\bar{\theta}$ is varied from $0°$ to $90°$. The calculations were performed with both the full-wave and the ray optics methods, and the results are shown in Figs. 7(a) and 7(b) for $k = 0.01$ and 0.1, respectively. The agreement between the two methods is excellent except for regions ($k = 0.1$ and TM polarization) where the absorbance per centimeter reaches extremely high values (>30 cm^{-1}). Thus in the regime where measurements are experimentally feasible (A cm$^{-1} < 10$ cm^{-1}), the discrepancy between the methods is minimal.

Finally the dichroic ratio, defined as the ratio of the TE and the TM absorbance values, is considered. The dichroic ratio is a measure of the angular orientation distribution of the molecules in the adlayer on the waveguide surface, and it is independent of the molecular concentration, c, in the ray optics approach. The dichroic ratio was calculated with both the full-wave and the ray optics models as described above. In Fig. 7(c) the relative error is displayed for $k = 0.01$. Excellent agreement between the two models is evident. In the same plot are included the results for the relative error calculated from expressions currently being used in the literature.[37] These results show a relative error of 5%, which can be explained by the lack of a cosine factor in the absorbance expressions reported by Lee and Saavedra.[37] In Fig. 7(d) we display the relative error for the case of $k = 0.1$. Again, the ray optics show good agreement with the wave model except in the angular region where the predicted absorbance values are extremely high.

5. Conclusions

We have derived straightforward expressions for calculating absorbance in typical planar waveguide geometries by the ray optics model. The accuracy of the approximations used in the ray optics approach has been assessed by comparison of results from absorbance calculations with those obtained with an exact electromagnetic wave approach. From this analysis, we conclude that in typical situations in which waveguide absorbance measurements are used
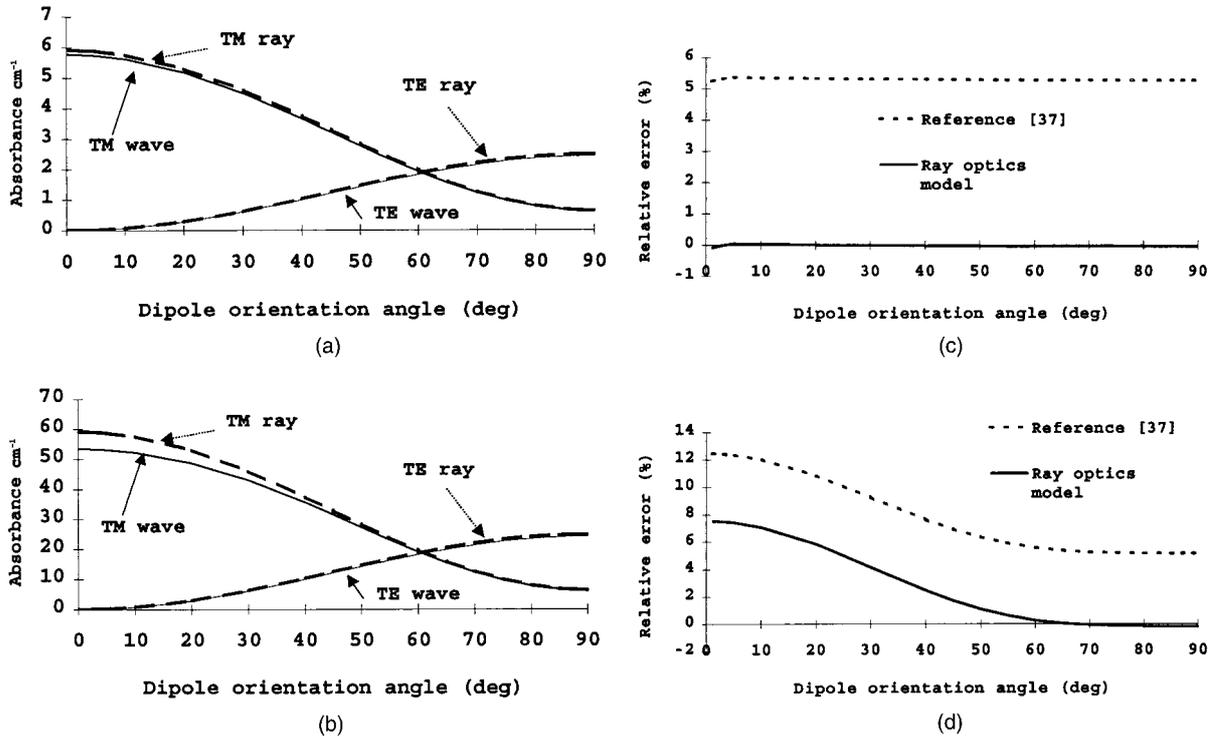
Fig. 7. Calculations for a dichroic adlayer with a variable dipole orientation angle, $\bar{\theta}$. The extinction coefficients (k_x, k_y, and k_z) are described in Eqs. (17) and (18). Absorbance values calculated by the ray optics (dashed curves) and the wave (solid curves) models for (a) $k = 0.01$ and (b) $k = 0.1$. Relative error of the dichroic ratio for the ray optics model and for expressions in Ref. [37] with (c) $k = 0.01$ and (d) $k = 0.1$. The parameters used in the calculations are wavelength $\lambda = 550$ nm, waveguide thickness $t = 400$ nm, waveguide index of refraction $n_w = 1.56$, substrate index of refraction $n_s = 1.46$, real part of the adlayer index of refraction $n_l = 1.33$, and cladding index of refraction $n_c = 1.33$.

to study organic thin films ($k_l/n_l \approx 10^{-1}$, $h/\lambda \approx 10^{-2}$), the ray optics model provides accurate results.

Appendix A: Dichroic Extinction Coefficients

Following Hopf and Stegeman,[44] the induced dipole, $\boldsymbol{p}$, associated with a normal mode is written as

$$\boldsymbol{p} = q\boldsymbol{l}, \qquad (A1)$$

with

$$\boldsymbol{l} = l\hat{\boldsymbol{e}}, \qquad (A2)$$

where l is the effective charge separation per unit length of q and $\hat{\boldsymbol{e}}$ is a unit vector in the direction of the induced dipole. The molecular polarizability tensor is given by

$$\bar{\alpha} = \frac{\boldsymbol{ll}}{m(\omega_o{}^2 - \omega^2 - i\omega\Gamma)}, \qquad (A3)$$

where ω_0 is the resonance frequency, Γ is the damping constant, and m is the characteristic mass. The extinction coefficient is linearly proportional to the imaginary part of the polarizability tensor through the relation

$$k_{ij} = \frac{\rho}{2\varepsilon_0} \operatorname{Im}\langle \bar{\alpha}_{ij} \rangle, \qquad (A4)$$

where ρ represents the volume molecular density and the brackets indicate an average over the molecular orientation distribution. Because of the symmetry considerations described below, it is preferable to represent the ensemble average in the polar coordinate system,

$$\langle f \rangle = \frac{\displaystyle\iint f(\theta, \phi) N(\theta, \phi) \sin(\theta) \mathrm{d}\theta \mathrm{d}\phi}{\displaystyle\iint N(\theta, \phi) \sin(\theta) \mathrm{d}\theta \mathrm{d}\phi}, \qquad (A5)$$

where $N(\theta, \phi)$ is the molecular orientation distribution.

1. Linear-Polarized Dipole

In the case of a linear dipole the Cartesian components are represented by

$$
\begin{pmatrix} l_x \\ l_y \\ l_z \end{pmatrix} =
\begin{pmatrix} \cos\phi & -\sin\phi & 0 \\ \sin\phi & \cos\phi & 0 \\ 0 & 0 & 1 \end{pmatrix}
\begin{pmatrix} \cos\theta & 0 & \sin\theta \\ 0 & 1 & 0 \\ -\sin\theta & 0 & \cos\theta \end{pmatrix}
\begin{pmatrix} 0 \\ 0 \\ l \end{pmatrix}
$$
$$
= \begin{pmatrix} \cos\phi \sin\theta \\ \sin\phi \sin\theta \\ \cos\theta \end{pmatrix} l. \qquad (A6)
$$

The orientation distribution of the dipoles in the x–y plane (the waveguide plane as shown in Fig. 3) is assumed to be isotropic; therefore

$$N(\theta, \phi) = N(\theta), \qquad (A7)$$

which gives

$$\langle l_x^2 \rangle = \langle l_y^2 \rangle = \frac{1}{2} l^2 \frac{\int \sin^2(\theta) N(\theta) \sin(\theta) d\theta}{\int N(\theta) \sin(\theta) d\theta}, \qquad (A8)$$

$$\langle l_z^2 \rangle = l^2 \frac{\int \cos^2(\theta) N(\theta) \sin(\theta) d\theta}{\int N(\theta) \sin(\theta) d\theta}, \qquad (A9)$$

$$\langle l_i l_j \rangle = 0, \qquad \text{for} \quad i \neq j. \qquad (A10)$$

It is common practice to express the dichroism in

2. Circular-Polarized Dipole

For two orthogonal dipoles, l_1 and l_2, their spatial orientation is described by a set of independent angular rotations (Euler angles):

$$\begin{pmatrix} l_x \\ l_y \\ l_z \end{pmatrix} = \begin{pmatrix} \cos\phi & -\sin\phi & 0 \\ \sin\phi & \cos\phi & 0 \\ 0 & 0 & 1 \end{pmatrix} \begin{pmatrix} 1 & 0 & 0 \\ 0 & \cos\theta & -\sin\theta \\ 0 & \sin\theta & \cos\theta \end{pmatrix}$$
$$\times \begin{pmatrix} \cos\alpha & -\sin\alpha & 0 \\ \sin\alpha & \cos\alpha & 0 \\ 0 & 0 & 1 \end{pmatrix} \begin{pmatrix} l_1 \\ l_2 \\ 0 \end{pmatrix}. \qquad (A17)$$

In the right-hand side of Eq. (A17), the first matrix applied to the dipole vectors represents a rotation in the plane of the dipoles. For a porphyrin molecule, this represents a rotation of the dipoles in the molecular plane. The second matrix implements a rotation on the polar angle θ. The third matrix applied to the vectors is a rotation on the azimuthal angle φ. The Cartesian components are then given by

$$\begin{pmatrix} l_x \\ l_y \\ l_z \end{pmatrix} = \begin{pmatrix} l_1(\cos\phi\cos\alpha - \sin\phi\sin\alpha\cos\theta) + l_2(-\cos\phi\sin\alpha - \sin\phi\cos\alpha\cos\theta) \\ l_1(\sin\phi\cos\alpha + \cos\phi\sin\alpha\cos\theta) + l_2(-\sin\phi\sin\alpha + \cos\phi\cos\alpha\cos\theta) \\ l_1(\sin\alpha\sin\theta) + l_2(\cos\alpha\sin\theta) \end{pmatrix}. \qquad (A18)$$

terms of an equivalent mean tilt angle. This angle is calculated by assuming a Dirac delta function for the polar dipole orientation distribution, $N(\theta)$

$$N(\theta) = \delta(\theta - \bar{\theta}), \qquad (A11)$$

therefore

$$\langle l_x^2 \rangle = \langle l_y^2 \rangle = \tfrac{1}{2} l^2 \sin^2(\bar{\theta}), \qquad (A12)$$

$$\langle l_z^2 \rangle = l^2 \cos^2(\bar{\theta}). \qquad (A13)$$

However, for a random distribution of polar tilt angles, $N(\theta) = 1$ is inserted into Eqs. (A8) and (A9) to get

$$\langle l_x^2 \rangle = \langle l_y^2 \rangle = \langle l_z^2 \rangle = (1/3) l^2. \qquad (A14)$$

These results allow the extinction coefficient for each Cartesian component to be expressed in terms of the extinction coefficient, k, of the randomly oriented ensemble of dipoles by

$$k_x = k_y = (3/2) k \sin^2(\bar{\theta}), \qquad (A15)$$

$$k_z = 3k \cos^2(\bar{\theta}). \qquad (A16)$$

At 54.74°, the so-called magic angle, the components of the extinction coefficient correspond to an isotropic medium, which means that $k_x = k_y = k_z$. Values of the mean tilt angle that are far from the magic angle indicate strong dichroism.

For an ensemble of circularly polarized molecules, the distribution along α is uniform. We also assume a uniform distribution (uniaxial) in the x–y plane. Under these assumptions, the molecular orientation distribution becomes

$$N(\theta, \phi, \alpha) = N(\theta), \qquad (A19)$$

which gives

$$\langle l_x^2 \rangle = \langle l_y^2 \rangle = \frac{1}{4} l^2 \frac{\int N(\theta)[1 + \cos^2(\theta)] \sin(\theta) d\theta}{\int N(\theta) \sin(\theta) d\theta}, \qquad (A20)$$

$$\langle l_z^2 \rangle = \frac{1}{2} l^2 \frac{\int N(\theta) \sin^2(\theta) \sin(\theta) d\theta}{\int N(\theta) \sin(\theta) d\theta}, \qquad (A21)$$

$$\langle l_x l_y \rangle = \langle l_x l_z \rangle = \langle l_y l_z \rangle = 0, \qquad (A22)$$

where the definition $l^2 \equiv l_1^2 + l_2^2$ is used.

Applying a simple consistency test for a random distribution, where all dipole orientations should be equally probable, we obtain

$$\langle l_x^2 \rangle = \langle l_y^2 \rangle = \langle l_z^2 \rangle = (1/3) l^2. \qquad (A23)$$

Again, by expression of the dichroism in terms of an equivalent mean angle

$$N(\theta) = \delta(\theta - \bar{\theta}), \qquad (A24)$$

the following expressions are obtained:

$$\langle l_x{}^2 \rangle = \langle l_y{}^2 \rangle = \tfrac{1}{4} l^2 [1 + \cos^2(\bar{\theta})], \qquad (A25)$$

$$\langle l_z{}^2 \rangle = \tfrac{1}{2} l^2 \sin^2(\bar{\theta}). \qquad (A26)$$

The extinction coefficients in each Cartesian component is then given by

$$k_x = k_y = (3/4)k[1 + \cos^2(\bar{\theta})], \qquad (A27)$$

$$k_z = (3/2)k \sin^2(\bar{\theta}). \qquad (A28)$$

As a final note, the factor f_i is defined as the ratio between the extinction coefficient in each Cartesian direction and the extinction coefficient for an ensemble of randomly oriented dipoles:

$$f_i \equiv \frac{k_i}{k}. \qquad (A29)$$

The definition is applied to both the linear- and the circular-polarized dipoles, and these factors are used in the calculations of dichroic absorption in Section 3.

References and Notes

1. J. D. Swalen, D. L. Allara, J. D. Andrade, E. A. Chandross, S. Garoff, J. Israelachvili, T. J. McCarthy, R. Murray, R. F. Pease, J. F. Rabolt, K. J. Wynne, and H. Yu, "Molecular monolayers and films," Langmuir **3,** 932–950 (1987).
2. M. Losche, "Protein monolayers at interfaces," Curr. Opin. Solid State Mater. Sci. **2,** 546–556 (1997).
3. A. Ulman, *An Introduction to Ultrathin Organic Films* (Academic, San Diego, 1991); A. Ulman, *Characterization of Organic Thin Films* (Butterworth-Heinemann, Stoneham, Mass., 1995).
4. C. Nicolini, "Supramolecular architecture and molecular bioelectronics," Thin Solid Films **285,** 1–5 (1996).
5. B. J. Ratner, "The engineering of biomaterials exhibiting recognition and specificity," J. Mol. Recog. **9,** 617–625 (1996).
6. L. Kang and R. E. Dessey, "Slab waveguides in chemistry," CRC Crit. Rev. Anal. Chem. **21,** 377–388 (1990).
7. T. E. Plowman, S. S. Saavedra, and W. M. Reichert, "Planar integrated optical methods for examining thin films and their surface adlayers," Biomaterials **19,** 341–355 (1998).
8. P. W. Bohn, "Localized optical phenomena and the characterization of materials interfaces," Ann. Rev. Mater. Sci. **27,** 469–498 (1997).
9. D. A. Stephens and P. W. Bohn, "Absorption spectrometry of bound monolayers on integrated optical structures," Anal. Chem. **61,** 386–390 (1989).
10. S. S. Saavedra and W. M. Reichert, "*In situ* quantitation of protein adsorption density by integrated optical waveguide attenuated total reflection spectrometry," Langmuir **7,** 995–999 (1991).
11. D. S. Walker, M. D. Garrison, and W. M. Reichert, "Protein adsorption to HEMA/EMA copolymers studied by integrated optical techniques," J. Colloid. Interface Sci. **157,** 41–49 (1993).
12. T. E. Plowman, M. D. Garrison, D. S. Walker, and W. M. Reichert, "Surface sensitivity of SiON integrated optical waveguides (IOWs) examined by IOW-attenuated total reflec-
tion spectrometry and IOW-Raman spectroscopy," Thin Solid Films **243,** 610–615 (1994).
13. D. M. Cropek and P. W. Bohn, "Surface molecular orientations determined by electronic linear dichroism in optical waveguide structures," J. Phys. Chem. **94,** 6452–6457 (1990).
14. L. Yang and S. S. Saavedra, "Chemical sensing using sol-gel derived planar waveguides and incicator phases," Anal. Chem. **67,** 1307–1314 (1995).
15. P. L. Edmiston and S. S. Saavedra, "Molecular orientation distributions in protein films. 4. A multilayer composed of yeast cytochrome c bound through an intermediate streptavidin layer to a planar supported phospholipid bilayer," J. Amer. Chem. Soc. **120,** 1665–1671 (1998); P. L. Edmiston, J. E. Lee, S. S. Cheng, and S. S. Saavedra, "Molecular orientation distributions in protein films. 1. Cytochrome c adsorbed to substrates of variable surface chemistry," J. Amer. Chem. Soc. **119,** 560–570 (1997); P. L. Edmiston, J. E. Lee, L. L. Wood, and S. S. Saavedra, "Dipole orientation distributions in Langmuir–Blodgett films by planar waveguide linear dichroism and fluorescence anisotropy," J. Amer. Chem. Soc. **100,** 775–784 (1996).
16. B. A. Bolton and J. R. Schere, "Raman-spectra and water-absorption of bovine serum-albumin," J. Phys. Chem. **93,** 7635–7640 (1989).
17. W. M. Reichert, J. T. Ives, P. A. Suci, and J. D. Andrade, "Excitation of fluorescent emission from solutions at the surface of polymer thin-film wave-guides—an integrated-optics technique for the sensing of fluorescence at the polymer-solution interface," Appl. Spectrosc. **41,** 636–640 (1987).
18. S. J. Choquette, L. Locasio-Brown, and R. A. Durst, "Planar wave-guide immunosensor with fluorescent liposome amplification," Anal. Chem. **64,** 55–60 (1992).
19. K. Itoh and A. Fujishima, "An application of optical waveguides to electrochemistry: construction of optical waveguide electrodes," J. Phys. Chem. **92,** 7043–7045 (1988); D. R. Dunphy, S. B. Mendes, S. S. Saavedra, and N. R. Armstrong, "The electroactive integrated optical waveguide: ultrasensitive spectroelectrochemistry of submonolayer adsorbates," Anal. Chem. **69,** 3086–3094 (1997).
20. J. S. Kanger, C. Otto, M. Slotboom, and J. J. Greve, "Waveguide Raman spectroscopy of thin polymer layers and monolayers of biomolecules using high refractive index waveguides," J. Phys. Chem. **100,** 3288–3292 (1996).
21. J. F. Rabolt, R. Santo, N. E. Schlotter, and J. D. Swalen, "Integrated-optics and Raman-scattering molecular orientation in thin polymer-films and Langmuir–Blodgett monolayers," IBM J. Res. Dev. **26,** 209–216 (1982); J. P. Rabe, J. D. Swalen, and J. F. Rabolt, "Order-disorder transitions in Langmuir–Blodgett films. 3. Polarized Raman studies of cadmium Arachidate using integrated optical techniques," J. Chem. Phys. **86,** 1601–1607 (1987).
22. S. S. Saavedra and W. M. Reichert, "Integrated optical attenuated total reflection spectrometry of aqueous superstrates using prism-coupled polymer waveguides," Anal. Chem. **62,** 2251–2256 (1990).
23. S. B. Mendes, L. Li, L. J. J. Burke, J. E. Lee, D. R. Dunphy, and S. S. Saavedra, "Broad-band attenuated total reflection spectroscopy of a hydrated protein film on a single mode planar waveguide," Langmuir **12,** 3374–3376 (1996).
24. J. J. Burke, "Propagation constants of resonant waves on homogeneous, isotropic slab waveguides," Appl. Opt. **9,** 2444–2452 (1970).
25. I. P. Kaminow, W. L. Mammel, and H. P. Weber, "Metal-clad optical waveguides: analytical and experimental study," Appl. Opt. **13,** 396–405 (1974).
26. J. Chilwell and I. Hodgkinson, "Thin-films field-transfer matrix theory of planar multilayer waveguides and reflection

from prism-loaded waveguides," J. Opt. Soc. Am. A **1,** 742–753 (1984).

27. J. F. Offersgaard, "Waveguides formed by multiple layers of dielectric, semiconductor, or metallic media with optical loss and anisotropy," J. Opt. Soc. Am. A **12,** 2122–2128 (1995).

28. A. J. Ghatak, K. Thyagarajan, and M. R. Shenoy, "Numerical analysis of planar optical waveguides using matrix approach," J. Lightwave Tech. **LT-5,** 660–667 (1987).

29. L. Li, "Determination of bound modes of multilayer for diffraction gratings of arbitrary profile, depth, and permittivity," J. Opt. Soc. Am. A **11,** 984–991 (1994).

30. G. L. Mitchell, "Absorption spectroscopy in scattering samples using integrated optics," J. Quantum Electron. **QE-13,** 173–176 (1977).

31. H. Nishihara, M. Haruna, and T. Suhara, *Optical Integrated Circuits* (McGraw-Hill, New York, 1989).

32. J. E. Midwinter, "On the use of optical waveguide techniques for internal reflection spectroscopy," IEEE J. Quantum Electron. **QE-7,** 339–344 (1971).

33. N. S. Kapany and J. J. Burke, *Optical Waveguides* (Academic, New York, 1972).

34. J. N. Polky and J. H. Harris, "Absorption from thin-film waveguides," J. Opt. Soc. Am. **62,** 1081–1087 (1972).

35. A. Reisinger, "Characteristics of optical guided modes in lossy waveguides," Appl. Opt. **12,** 1015–1025 (1973).

36. G. Stewart and B. Culshaw, "Optical waveguide modeling and design for evanescent field chemical sensors," Opt. Quantum Electron. **26,** S249–S259 (1994).

37. J. E. Lee and S. S. Saavedra, "Molecular orientation in heme protein films adsorbed to hydrophilic and hydrophobic glass surfaces," Langmuir **12,** 4025–4032 (1996); J. E. Lee and S. S. Saavedra, "Molecular orientation in adsorbed cytochrome c films by planar waveguide linear dichroism," in *Proteins and Interfaces II: Fundamentals and Applications*, T. A. Horbett and J. L. Brash, eds., ACS Symposium Series **602,** 269–279 (1995).

38. W. H. Press, S. A. Teukolsky, W. T. Vetterling, and B. P. Flannery, *Numerical Recipes* (Cambridge, New York, 1992).

39. Expressions for the Goos–Hänchen shift that appear in Ref. 22, which were taken from T. Hirshfeld, Appl. Spectrosc. **31,** 243 (1977), are incorrect. The correct expressions are given, for instance, in Ref. 31.

40. N. J. Harrick, *Internal Reflection Spectroscopy* (Wiley, New York, 1967).

41. F. M. Mirabella, Jr. and N. J. Harrick, *Internal Reflection Spectroscopy: Review and Supplement* (Harrick Scientific Corporation, New York, 1985).

42. H. A. Macleod, *Thin-Film Optical Filters* (Macmillan, New York, 1986).

43. F. Horowitz and S. B. Mendes, "Envelope and waveguide methods: a comparative study of PbF_2 and CeO_2 birefringent films," Appl. Opt. **33,** 2659–2663 (1994).

44. F. A. Hopf and G. I. Stegeman, *Applied Classical Electrodynamics, Vol. I: Linear Optics* (Krieger, Malabar, Fla., 1985).